Film Cooling Performance in a Transonic High-Pressure Vane: Decoupled Simulation and Conjugate Heat Transfer Analysis

Available online at www.sciencedirect.com

ScienceDirect

Energy Procedia 45 (2014) 1126 – 1135

Energy Procedia

68th Conference of the Italian Thermal Machines Engineering Association, ATI2013

Film cooling performance in a transonic high-pressure vane: decoupled simulation and conjugate heat transfer analysis

Massimiliano Insinna, Duccio Griffini, Simone Salvadori*, Francesco Martelli

DIEF, Department of Industrial Engineering Florence, University of Firenze, via di Santa Marta 3, 50139 Firenze, Italia

Abstract

The continuous demand for increased performance and reliability of gas turbines leads to the improvement of prediction tools. Having regard to the effects of heat transfer on the residual life of gas turbine components, it is necessary to achieve a high level of accuracy in the evaluation of thermal loads. Computational fluid dynamics is able to provide reliable data in a limited lapse of time. In this paper, the numerical analysis of the cooled vane of the MT1 high-pressure turbine stage is presented. A grid dependence analysis based on the evaluation of the aero-thermal characteristics of the vane has been performed. Turbulence is modeled using the k_T-k_L-ω method whose performance in this kind of configuration is rarely debated in the scientific literature. Model parameters have been tuned to match the experimental data. The final objective of the present activity is to assess the capability of numerical methods to deal with an annular, transonic high-pressure vane with a realistic film cooling configuration. Adiabatic effectiveness, heat transfer coefficient and net heat flux reduction distributions have been evaluated, the latter providing relevant information on the performance of the cooling system. The coupled fluid-solid simulation of the cooled configuration has also been performed to evaluate the impact of conjugate heat transfer on the prediction of thermal loads. Results show a non-negligible difference in the wall temperature evaluation between the decoupled and the coupled approach, mainly caused by the heat conduction in the solid.

Selection and peer-review under responsibility of ATI NAZIONALE

Keywords: High-Pressure Vane, Film Cooling, Transition Modeling, Grid Dependence, Conjugate Heat Transfer

* Corresponding author. Tel.: +39-055-4796-330; fax: +39-055-4796-342.
E-mail address: simone.salvadori@unifi.it

1876-6102
Selection and peer-review under responsibility of ATI NAZIONALE
doi:10.1016/j.egypro.2014.01.118

Nomenclature

C	Chord [m]; transition model constants [-]
k_T	Turbulent kinetic energy [m^2/s^2]
k_L	Laminar kinetic energy [m^2/s^2]
$\dot{q}$	Heat flux [W/m^2]
T	Temperature [K]
X	Axial coordinate [m]
y^+	Non-dimensional wall distance [-]

Subscripts

0	Stagnation value
ax	Axial
aw	Adiabatic wall
c	Coolant
main	Main-flow
rec	Recovery
w	Wall

Greek

η	Effectiveness [-]
ω	Specific dissipation rate [1/s]

1. Introduction

Numerical simulation of a cooled, transonic High-Pressure Vane (HPV) is one of the most challenging topics in the Computational Fluid Dynamics (CFD) field. It includes the analysis of a transitional flow governed by geometrical parameters (cooling holes shape, diameter and pitch) and by non-negligible compressibility effects. The potential interaction between the vane and the rotating blades also modifies the boundary layer development on the rear suction side (SS) of the vane.

Although the usage of Large-Eddy Simulation (LES) for heat transfer analysis in HPV has been recently documented by Gourdain *et al.* in [1], such a demanding approach is far from being the first choice during the design procedure of next-gen aero-engines. A less demanding approach based on the Detached-Eddy Simulation (DES) methodology has been suggested by Takahashi *et al.* [2] in comparison with an Unsteady Reynolds-Averaged Navier-Stokes (URANS) calculation with the *k-ε-v²-f* transition model by Lien and Kalitzin [3]. Selected methodologies show good results in the estimation of a simplified leading edge configuration with showerhead cooling, but DES performance in a realistic high-pressure turbine (HPT) environment has still to be analyzed.

Heat transfer in cooled HPV is usually analyzed considering either steady or unsteady simulations where turbulence is modeled using two-equation approaches. In this regard, Adami *et al.* [4] and Montomoli *et al.* [5] presented several steady analyses of cooled vanes. Results demonstrate that the *k-ω* model by Wilcox [6] is able to reproduce the Nusselt number distribution on the blade surface with reasonable accuracy. In [5] an in-house methodology for the Conjugate Heat Transfer (CHT) analysis is also presented and validated, and an improvement in the Nusselt number evaluation on the rear suction side of the vane is demonstrated. It must be underlined that a grid dependence analysis is missing and that improved accuracy is also expected when modelling boundary layer transition.

Luo and Razinsky [7] presented the numerical study of an internally cooled vane using a CHT approach and the *k-ε-v²-f* transition model, whose performance was previously tested in comparison with fully turbulent approaches. Although the results show good agreement with the available experimental data in terms of wall temperature, heat

transfer coefficient (HTC) and Nusselt number, the vane geometry used in [7] is equipped with internal cooling channels only, and then no information is provided on film cooling effects, whose presence governs the bypass transition mechanism in HPV.

One of the most interesting papers including CHT in a cooled HPV configuration is presented by He and Oldfield [8]. An unsteady approach for CHT based on the Fourier analysis of the fluid/solid interface temperature is successfully applied to a HPV, but it must be underlined that also in this case a fully turbulent approach is considered and then boundary layer transition is completely missed. This result highlights again the importance of transition modelling when heat transfer is studied.

The present activity is mainly devoted to assess the capability of RANS transition modelling to deal with a heat transfer problem on a realistic film-cooled vane configuration and to point out the physical effects due to the introduction of thermal conductivity of metal component. The test case selected for the numerical campaign includes internal cooling channels and a multi-row film cooling configuration. Grid dependence study is proposed considering relevant parameters in turbomachinery analysis. Turbulence is modelled using the k_T-k_L-ω model by Walters and Cokljat [9], rarely applied to three-dimensional heat transfer problems. A model assessment has been performed and a new set of constants is proposed. Once the decoupled analysis (limited to the fluid domain) has been completed, a conjugate approach for the fluid/solid interaction has been considered: the comparison between the results obtained using the two methods provides relevant information on their respective capabilities.

2. Description of the test case

The test case used for the numerical activity is the vane of the MT1 high-pressure stage. This is an un-shrouded, high-pressure research turbine designed by Rolls-Royce and tested in the Isentropic Light Piston Facility (ILPF) by QinetiQ [10][11]. MT1 is widely used for unsteady analysis of high-pressure turbine stages both in cooled and un-cooled configurations (see [4][5][8][12]). The stage, composed by 32 vanes and 60 blades, has been tested in a cooled configuration with uniform inlet conditions during the Turbine Aero-Thermal External Flows (TATEF) project funded by the European Commission. The Reynolds number, based on the true chord of the Nozzle Guide Vane (NGV) and evaluated at the NGV outlet which is positioned at the stage stator-rotor interface, is about 2.75E+06 while the value of the isentropic exit Mach number is around 0.942.

The cooling system is limited to the NGV, as well as the computational domain of the present research. Air supply is assured by two plenum channels positioned inside of the blade. The diameter of the front and of the rear plenum is 10mm and 7mm respectively. Stagnation pressure is different between each plenum, leading to different coolant mass flows. Coolant reaches the vane surface through six rows of cylindrical holes: for each plenum, two rows are placed on the pressure side (PS) while a single row protects the suction side. The internal diameter of injection channels is 0.6mm and all the rows have a span-wise pitch of 1.8mm. The pressure side double row has an axial separation of 1.56mm. All the cooling rows are characterized by an inclination angle of 50deg with respect to the local tangent on the vane surface. The nominal cooling non-dimensional parameters are reported in [10] by Chana and Mole. Heat transfer measurements and pressure distributions along the surface of the vane are available from the experimental campaign. The vane operating conditions are summarized in Table 1.

Table 1. Vane boundary conditions (values are non-dimensional with respect to inlet stagnation conditions of the main-flow).

	Inlet	Plenum 1	Plenum 2	Wall	Outlet
Mean Total Pressure [-]	1.	1.365	1.061		
Mean Total Temperature [-]	1.	0.645	0.645		
Mean Turbulence Level [%]	6.	5.	5.		
Mean Turbulent Length Scale [m]	0.008	0.0004	0.0004		
Mean Metal Temperature (for isothermal calculations) [-]				0.65	
Mean Static Pressure [-]					0.565

3. Numerical approach and simulation matrix

Numerical simulations on hybrid unstructured grids have been performed using a steady approach with the commercial code ANSYS Fluent®. The transitional k_T-k_L-ω model by Walters and Cokljat [9] has been selected for the turbulence closure. A second-order accurate upwind discretization has been applied in space, while gradients are reconstructed with the Green-Gauss node based approach. The SIMPLE scheme has been used for the pressure-velocity coupling.

For sake of clarity all the performed simulations are summarized in Table 2. Different phases can be individuated, each finalized to a different type of analysis. The first part of the work is dedicated to a grid dependence analysis and leads to the choice of the mesh that will be used for subsequent simulations. The second part consists in the assessment of the transition model: several calculations have been performed varying some of the parameters of the model itself in order to reach the better reproduction of the experimental data. Afterwards the performance of the cooling system has been evaluated in terms of Heat Transfer Coefficient, adiabatic effectiveness (η_{aw}) and Net Heat Flux Reduction (NHFR) respectively defined in equations 1, 2 and 3. Finally, the thermal field inside the metal of the vane has been analyzed by means of a CHT simulation.

$$HTC = \frac{\dot{q}_w}{T_{rec,main} - T_w} \tag{1}$$

$$\eta_{aw} = \frac{T_{rec,main} - T_{aw}}{T_{rec,main} - T_{0c}} \tag{2}$$

$$\mathrm{NHFR} = \frac{\dot{q}_{w,\text{un-cooled}} - \dot{q}_{w,\text{cooled}}}{\dot{q}_{w,\text{un-cooled}}} = 1 - \frac{\dot{q}_{w,\text{cooled}}}{\dot{q}_{w,\text{un-cooled}}} \tag{3}$$

The computational domain includes the whole fluid region, i.e. the external flow, the coolant interior channels and the supply plenums, colored in blue in Fig. 1a. Inlet and outlet sections are placed respectively about $0.65C_{ax}$ upstream of the leading edge and about $0.15C_{ax}$ downstream of the trailing edge. The inlet sections of the cooling flow are located on the side of the external end-wall while the lower end is closed off.

Total pressure, total temperature, turbulence level, turbulent length scale and flow direction have been imposed on inlet sections for all the simulation. Zero laminar kinetic energy has been imposed on the inlet sections of both main-flow and plenums. The outlet section of the domain is located in correspondence of the stator/rotor interface and a static pressure map, obtained from the time-averaged solution of a previously performed unsteady simulation of the MT1 stage (see [12]), has been imposed to reproduce the radial and tangential gradients of the flow. All the thermal boundary conditions on the surfaces of vane (fluid domain) and end-walls are summarized in Table 2, while for the CHT analysis the vane regions at hub and shroud of the solid domain have been set as adiabatic.

Table 2. Simulation matrix.

Type of analysis	Geometry	Domain	Vane surface thermal condition	End-walls thermal condition	n° of runs
Grid sensitivity	cooled	fluid	T_w = 315 K	T_w = 315 K	4
Transition model assessment	cooled	fluid	T_w = 315 K	T_w = 315 K	13
η_{aw}	cooled	fluid	adiabatic	adiabatic	1
NHFR and HTC	cooled	fluid	T_w = 315 K	T_w = 315 K	1
NHFR	un-cooled	fluid	T_w = 315 K	T_w = 315 K	1
Thermal field in metal	cooled	fluid/solid	coupled	adiabatic	1

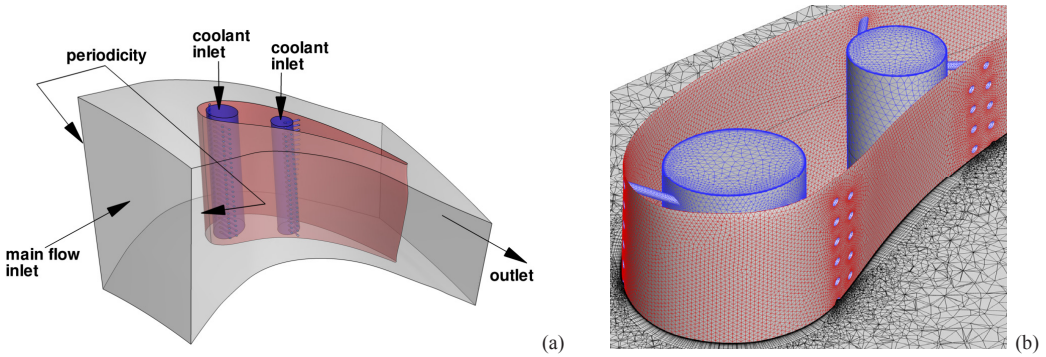

Fig. 1 (a) Schematic of the computational domain; (b) view of the grid (15M elements).

4. Grid dependence analysis

The geometry of a film-cooled vane is characterized by large variations of characteristic lengths, from cooling channels diameter to blade chord. This implies that very different length scales of the flow are present, and then grid generation must be considered a crucial issue in the simulation of film-cooled components. A grid dependence analysis is the only way to limit the computational cost of the numerical campaign without any influence on the accuracy of the obtained results. For that reason a grid dependence analysis has been carried out using hybrid unstructured grids generated with the commercial software Centaur™. Prismatic layers are used in the near wall region to better reproduce boundary layer development while tetrahedral elements are used to fill the remaining volume. The unstructured nature of the mesh allows obtaining local refinements where necessary, i.e. in the cooling channels and in the cross-flow zone between cooling flow and mainstream, as it is possible to observe in Fig. 1b.

Four different grids have been generated consisting of about 4M, 8M, 15M and 28M elements whose main characteristics are reported in Table 3. The number of circumferential divisions of the cooling channels and the maximum element dimension on the vane surface have been limited to respectively increasing values moving from 4M to 28M elements. The presence of 30 prismatic layers adjacent to the vane walls has been enforced for all the investigated meshes in order to obtain the same accuracy in the discretization of the boundary layer. The number of prismatic layers has been maintained unchanged also in channels and plenums, as well as the expansion ratio between each layer. For the first three layers the expansion ratio is 1.0 while it changes to 1.2 from the fourth to the tenth and to 1.25 for the remaining prisms. The height of the first prismatic cell is coherent with a low Reynolds approach, as demonstrated by the y^+ values shown in Table 3.

Table 3. Grid properties and required computational time.

grid	domain type	n° of tetrahedra (x 10^6)	n° of prisms (x 10^6)	average y^+	maximum y^+	s/iteration (24 cores)
4M	fluid	1.96	1.96	0.45	2.22	8.6
8M	fluid	4.30	3.80	0.47	1.20	10.1
15M	fluid	6.70	8.50	0.47	1.38	17.6
28M	fluid	10.1	17.9	0.45	1.49	30.6

Some results of the grid dependence analysis are shown in Fig. 2. Mach number distributions are shown in Fig. 2a at various grid resolutions. All the grids are almost equivalent except for the coarse one (4M) that shows a different behavior immediately downstream of the last cooling row on the suction side. Some differences between the grids are also present downstream of the cooling holes (vertical dashed lines in the image), where peaks are filtered out in the coarser versions. A good agreement with the experimental data is achieved, except in the terminal part of the suction side due to the time-averaged exit condition which is not able to mimic the real effect of stator-rotor interaction. Fig. 2b shows the trend of the mass flows of the mainstream and of the two plenums. Values are normalized with respect to the result obtained using the 28M grid. All the flow rates show an asymptotic behavior

increasing the element number. Although the higher discrepancies are individuated on the coolant mass flows, variations of 2.6% for the front plenum and 3.1% for the rear one between the 15M grid and the 28M grid are considered acceptable, especially considering that computational costs are doubled.

In Fig. 2c a detailed view of the secondary flow structures downstream of a cooling hole located at mid-span on the suction side is shown. The section is obtained about six diameters downstream to the hole itself. The classical kidney vortex structure is not present in the solution obtained with the 4M grid, while in the 8M grid it is poorly defined. In the 28M grid it appears to be sufficiently well defined, but also in the 15M grid it shown very similarly.

After the grid dependence analysis it could be concluded that evaluating the adequacy of a grid relying only on aerodynamic parameters like the isentropic Mach number distribution would have been incorrect, because it would lead to select a grid that filters out some of the flow structures that drive heat transfer. The analysis demonstrates that doubling the computational cost from 15M elements to 28M (Table 3) does not introduce significant improvements in the accuracy of the solution, therefore for the subsequent simulations the 15M grid is used.

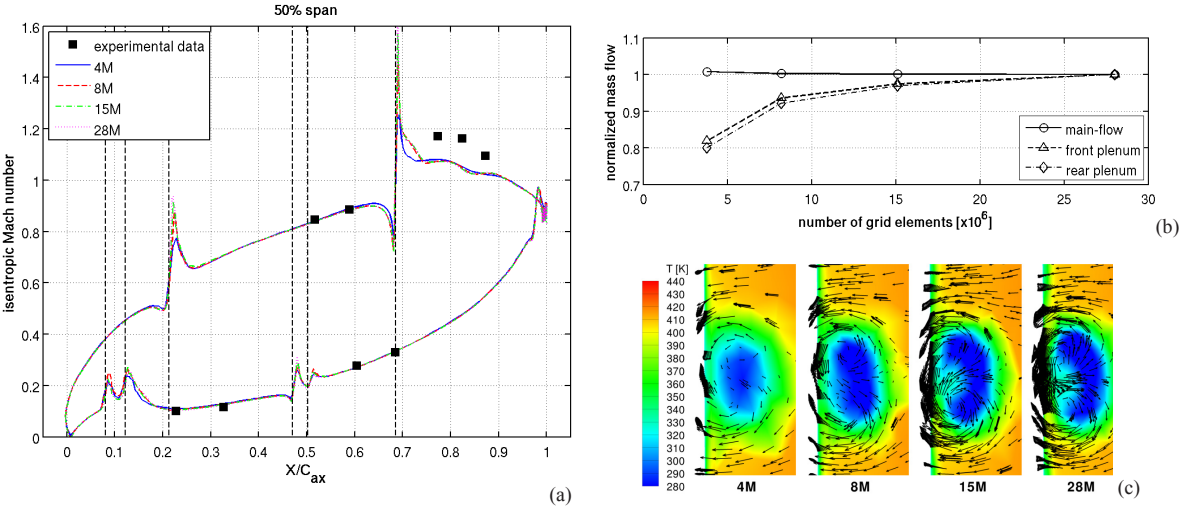

Fig. 2 Grid dependence of: (a) isentropic Mach number distribution along the vane; (b) normalized mass flow of mainstream, front and rear plenum. (c) View of the kidney vortices downstream of a cooling hole on suction side at mid-span as a function of the number of grid elements.

5. Assessment of the k_T-k_L-ω model

After selecting the appropriate grid, the assessment of the turbulence model has been performed. As stated before the k_T-k_L-ω model by Walters and Cokljat [9] has been selected for the analysis. It is based on the k-ω structure and is able to predict both natural and bypass transition mechanisms. A third transport equation for laminar kinetic energy k_L has been added to predict the behavior of the low-frequency velocity fluctuations in the pre-transitional zone of the boundary layer. The k_T-k_L-ω model is not fully based on empirical correlations like other models but it is conceived on a phenomenological approach that makes it probably more suitable for engineering evaluations. However the complexity of the physics that is the basis of transition process implies the use of a large number of model constants. For the assessment proposed in this work four parameters have been modified with respects to the original set of 27 proposed by Walters and Cokljat: $C_{R,NAT}$, $C_{NAT,crit}$, C_λ and C_R. For the definitions of these parameters refer directly to [9]. The choice of these parameters has been dictated by their role in the model. In fact, they control directly both natural and bypass transition and also the turbulence production term driven by strain rate.

Thirteen runs have been performed varying the selected parameters. For sake of brevity Table 4 summarizes only the sets of parameters that have shown the most significant results. Experimental data about Nusselt number along the mid-span of the vane has been considered for the model assessment. Nusselt number is defined coherently with

experimental data and is based on the axial chord of the vane and on the thermal conductivity of the air measured at the stagnation temperature of the main-flow at the inlet of the domain.

Looking at Fig. 3a, with the original constants (continuous black line) non-negligible discrepancies are present with respect to the experimental data. Nusselt number in the terminal part of the pressure side is completely miss-predicted since CFD results provide an opposite behavior with respect to experiments. Furthermore, downstream of the first cooling row along the suction side a non-physical flat Nusselt number behavior is observed between $0.28 < X/C_{ax} < 0.53$. Since experimental sensors are quite distant it is not easy to state the real behavior of the Nusselt number but, it is reasonable to believe that, due to the interaction between cooling jets and mainstream, turbulent structures are created immediately downstream of the row. Consequently a peak of heat transfer would be expected.

Fig. 3a also reports results from cases named SET1, SET2 and SET3. The unphysical behavior showed between $0.22 < X/C_{ax} < 0.53$ is no more present and a unique peak appears in this zone for the modified configurations. SET1 and SET3 have an opposite behavior on pressure and suction side with respect to the experimental data. In fact SET1 predicts more accurately the Nusselt number along the rear part of the pressure side and overestimates the heat transfer along the suction side while SET3 is closer to the experimental data along the suction side and underestimates the Nusselt number in the terminal part of the pressure side. SET2 is a good compromise over the entire vane and for this reason it has been chosen as the definitive setting for all the subsequent simulations.

To compute NHFR the simulation of the un-cooled geometry is also necessary and the selected set of modified parameters has been used. Grid has been generated with the same settings of the 15M grid of the cooled case. Results are shown in Fig. 3b: the new set of constants allows obtaining a better estimation of Nusselt number along the vane mid-span, if compared with the standard parameters. This is probably due to a better estimation of the overall turbulence production, which determines the heat transfer coefficient near the trailing edge. Another aspect can be highlighted from Fig. 3b, concerning the position of the transition initiation along the suction side. Although both the modified model and the original one are not able to reproduce correctly the transition point along the suction side, both of them move the transition position downstream with respect to the cooled case (vertical line in Fig. 3b). This result is physically correct because in the un-cooled case the turbulent production induced by the cross flow interaction between main-flow and cooling jets is absent.

Table 4. Test matrix for the transition model assessment (bolded values are modified with respect to the original model). See Walter and Cokljat [9] for the definition of the parameters. Note that $C_{NAT,crit}$ loses its meaning when $C_{R,NAT} = 0$.

RUN ID	$C_{R,NAT}$	$C_{NAT,crit}$	C_{λ}	C_R
Original model	0.02	1250	2.495	0.12
SET1	**0.00**	-	2.495	**0.60**
SET2	**0.00**	-	**2.200**	**0.80**
SET3	**0.00**	-	**1.800**	**1.40**

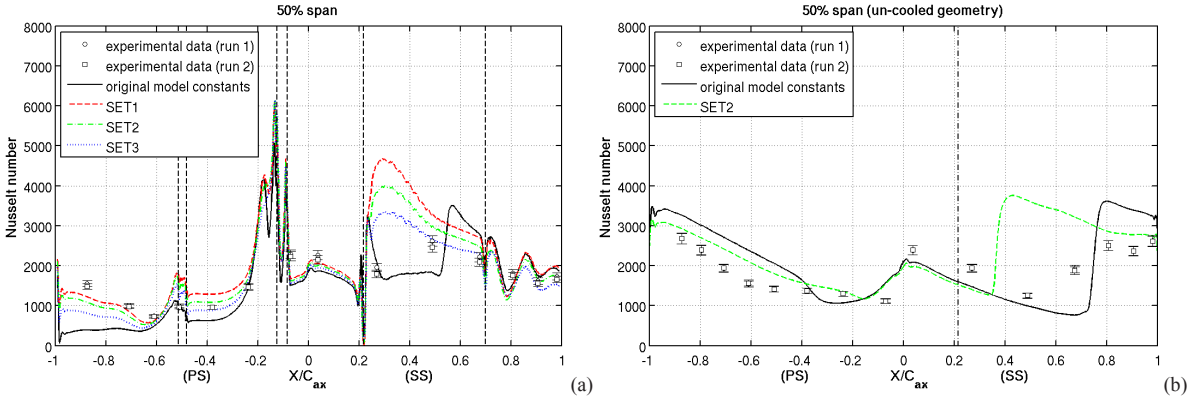

Fig. 3 (a) Cooled case: comparison of measured Nusselt number and CFD results with original and modified model constants (see Table 4); (b) Un-cooled case: comparison between the Nusselt number calculated with default and selected modified constants.

6. Film cooling performance

In this section the results of the decoupled simulations are shown and commented. The performance of the cooling system are discussed in terms of heat transfer coefficient, adiabatic effectiveness and net heat flux reduction.

Fig. 4a and Fig. 4b show the distribution of η_{aw} along the vane surface. From the behavior of this quantity the covering effect guaranteed by the cooling system can be observed. Effectiveness is zero on the vane leading edge since no cooling holes are present. Low values of η_{aw} (between 0. and 0.3) are present between the first and the second row of holes on the suction side: that result demonstrates that the covering effect provided by the first row along the suction side is weak. Furthermore, low values of η_{aw} (below 0.1) are present immediately downstream of the first couple of cooling rows on the pressure side: differently from the suction side, the extension of the uncovered zone on the pressure side is quite short and is followed by a zone where η_{aw} reaches values between 0.35 and 0.5. The weakly covered zones evidenced on suction and pressure side are due to the contemporary presence of a high blowing ratio and the particular geometrical configuration of the cooling holes. In fact, as stated in the description of the test rig, all the cooling rows are characterized by an inclination angle of 50deg with respect to the local tangent to the vane surface. This value is probably too high for a cylindrical hole working under high blowing ratio conditions and leads to high jet penetration and to the lift off of the coolant. The reattachment of the coolant along the vane happens after a relatively short distance along the pressure side because of the concave shape of the surface, while along the suction side, the convex shape of the surface is unfavorable and coolant appears to remain detached and to move parallel to the surface for a large zone. Reattachment is less defined with respect to the one on the pressure side and happens mainly thanks to turbulent diffusion. The negative effects of the lifting of the coolant are clearly evident from Fig. 4c and Fig. 4d, where HTC is shown. A remarkable increase of HTC is present downstream to the first rows, meaning that the detached coolant flow promotes mixing between main and cooling flow. The second cooling rows both on pressure and suction side provide a better coverage of the surface with respect to the first rows without lift off. The coverage is more effective on the pressure side due to the fact that two staggered holes are present and a larger amount of cooling flow is injected with respect to the suction side.

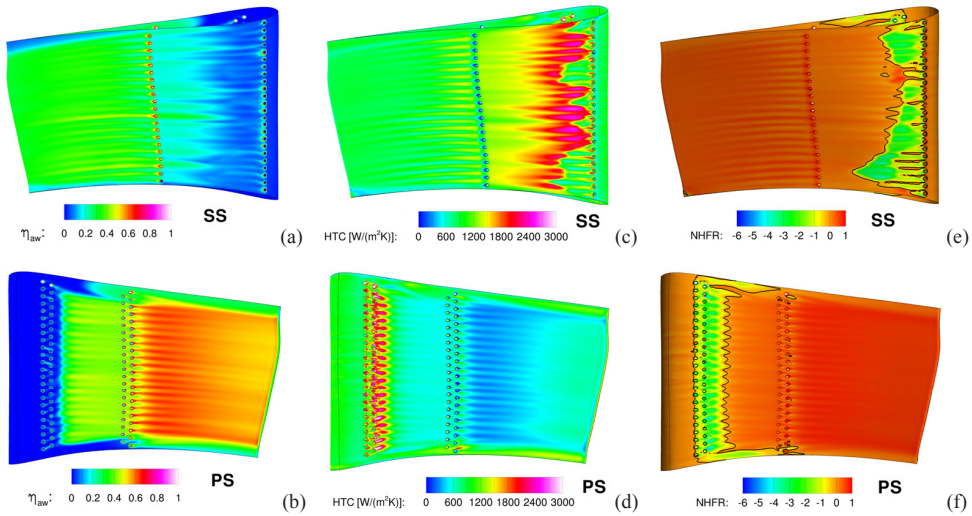

Fig. 4 (a-b) adiabatic effectiveness; (c-d) heat transfer coefficient; (e-f) net heat flux reduction.

The overall effects of the cooling system can be summarized by using NHFR. CFD simulations allow to have the local heat flux along the walls therefore the direct calculation of NHFR is possible (as indicated in equation 3), instead of using the classical experimental definition. To allow the calculation of the map of NHFR wall heat fluxes for the un-cooled case have been interpolated onto the grid of the cooled geometry. As shown in Fig. 4e and Fig. 4f large zones of negative NHFR (bounded by the black line at NHFR = 0) are present and are located mainly

downstream to the first cooling rows. This means that the weak covering of the vane surface and the increase of HTC lead to raise the heat flux entering the vane, inducing a detrimental effect of the cooling system. Another aspect that emerges from the visualization of NHFR is that two streaks of increased heat flux are induced by the presence of the cooling system in proximity of hub and shroud. This is again due to the contemporary presence of an almost null η_{aw} (no cooling holes are present at these span-wise positions) and of the increase of HTC promoted by the blockage effect generated by the cooling flow that tends to increase the velocity of the main-flow. Moreover in these zones the formation of secondary vertical structures (i.e. corner vortices) has started and this add a contribution to the local increase of HTC.

7. CHT analysis

A CHT simulation has been performed on the cooled geometry in order to consider the effects introduced by thermal conduction within the vane. Coherently with the experimental campaign, thermal conductivity of the material of the vane has been set referring to the Dural alloy (147 W/(m·K)). The computational mesh of the solid part has been created together with the 15M mesh of the fluid, and then characteristic dimensions of the elements are comparable between solid and fluid domains. Fluid/solid interface is conformal to avoid interpolation errors. The entire domain is composed by about 19.6M elements with 4.6M tetrahedral elements in the solid part.

Fig. 5 shows the results of the CHT analysis in terms of non-dimensional thermal field (a-b) and percentage difference of the external surface temperature of the vane (c-d), choosing T_{aw} as reference. The introduction of the solid part leads to very important changes in the surface temperature of the vane (ΔT between -20% and 10%). As expected, heat sink effects due to the internal convection are evident around plenums and channels. In fact heat is removed internally as demonstrated by the radial temperature gradients on the plenums, leading to the reduction of the surface temperature upstream of the second cooling row on the pressure side (ΔT between -5% and 0%).

Internal heat transfer from metal to fluid has a negative effect in the terminal part of the pressure side ($\Delta T \approx$ 10%). Going back to Fig. 4b, a strong coverage is guaranteed by the cooling system after the second rows along the pressure side. This aspect could appears beneficial if observing only the results of the decoupled analysis, as demonstrated also by NHFR (Fig. 4f), but introducing heat conduction within the vane the high effectiveness becomes a disadvantage (Fig. 5c and Fig. 5d). In fact, fluid exiting from the second couple of cooling holes along the pressure side has been heated internally and increases the surface temperature of the vane by external convection. On the contrary, temperature variations on the vane rear suction side (Fig. 5c) are less important. It can be also concluded that in the region between the first and the second row the cooling system is effective (ΔT between -10% and 0% on the suction side, between -20% and 0% on the pressure side), nevertheless that result is not ascribable to the coolant flow exiting the holes but to the heat sink effect of the first plenum in the leading edge region. These considerations highlight the importance of CHT analysis in the estimation of temperature of metallic components.

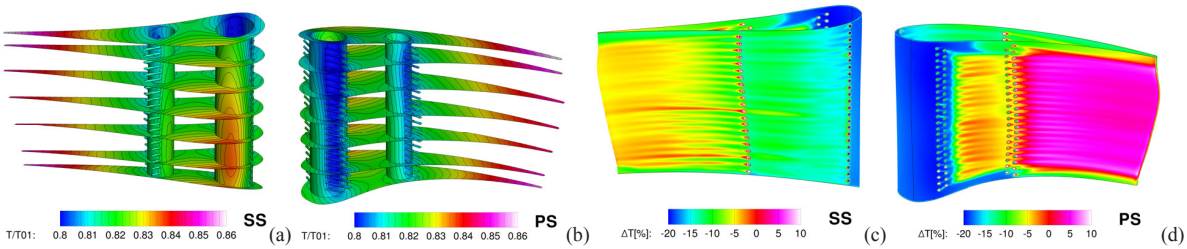

Fig. 5 (a-b) thermal field; (c-d) temperature difference between CHT and adiabatic case along the external surface of the vane.

8. Concluding remarks

Film cooling performance on a high-pressure research transonic turbine vane has been analyzed by means of decoupled and conjugate heat transfer simulations. An important part of the work has been dedicated to grid dependence analysis that allowed understanding how spatial discretization influences the results on a domain where very different geometrical length scales are present. The choice of the coarsest grid (8M elements) that shows an insensitive behavior from the point of view of pure aerodynamics, e.g. isentropic Mach number distribution, demonstrated to be inadequate for a heat transfer analysis because of some flow phenomena are filtered out by the grid resolution. In general it can be said that a finer discretization is needed with respect to a pure aerodynamics analysis in order to take into account small scale flow phenomena that locally drives heat transfer.

The transitional k_T-k_L-ω model used for the simulations, rarely applied in literature to this kind of problems, has shown promising results in reproducing experimental data on this geometry, where fully turbulent models fail. This transition model is more physics-based with respect to other empirical models available in literature and it is more adequate for a calibration based on the observation of flow phenomena, as shown in section 5.

The analyzed cooling system has shown some problems due to the lift off of the cooling jets exiting from the first plenum. In fact an increase of HTC due to the separation of the jets from the vane surface and the consequent enhanced mixing with the main-flow has been pointed out. A deeper comprehension of the heat transfer phenomena has been allowed by adding the solid domain of the vane in the analysis, demonstrating the importance of performing CHT simulation for the estimation of the effective performance of a cooling system. In fact adiabatic effectiveness gives clear information about the covering effect but could lead to misunderstand real effects of the cooling system. Well covered zones of the vane according to η_{aw} could result heated up by the coolant itself when the heat conduction in the solid part is considered: in fact, coolant increases its temperature due to the convection that happens within the internal passages of the cooling system.

Acknowledgements

The European Commission and the Brite-EuRam TATEF project (BRPR-CT97-0519) consortium are acknowledged. The authors would also like to acknowledge Dr. K.S. Chana from the University of Oxford for the support provided.

References

[1] Gourdain N, Gicquel LYM, Collado E. Comparison of RANS simulation and LES for the prediction of heat transfer in a highly loaded turbine guide vane. Proc. of the Ninth European Conference on Turbomachinery – Fluid Dynamics and Thermodynamics 2011, March 21-25, Istanbul, Turkey, Paper No. B235.

[2] Takahashi T, Funazaki K, Salleh HB, Sakai E, Watanabe K. Assessment of URANS and DES for prediction of leading edge film cooling. J Turbomach 2012, 134.

[3] Lien FS, Kalitzin G. Computations of transonic flow with the v^2-f turbulence model. Int. J. Heat Fluid Flow 2001, 22(1): 53–61.

[4] Adami P, Martelli F, Chana KS, Montomoli F. Numerical predictions of film cooled NGV blades. Proc. of IGTI, ASME Turbo Expo 2003 June 16-19, Atlanta, Georgia, USA, Paper No. GT-2003-38861.

[5] Montomoli F, Adami P, Della Gatta S, Martelli F. Conjugate heat transfer modelling in film cooled blades. Proc. of IGTI, ASME Turbo Expo 2004, June 14-17, Vienna, Austria, Paper No. GT-2004-53177.

[6] Wilcox DC. Turbulence Modeling for CFD. DCW Industries Inc. 1993

[7] Luo J, Razinsky EH. Conjugate heat transfer analysis of a cooled turbine vane using the V2F turbulence model. J Turbomach 2007, 129(4):773-781.

[8] He L, Oldfield MLG. Unsteady conjugate heat transfer modeling. J Turbomach 2011, 133.

[9] Walters DK, Cokljat D. A three-equation eddy-viscosity model for Reynolds-averaged Navier-Stokes simulations of transitional flow. J Fluids Engineering 2008. 130(4)

[10] Chana KS, Mole AH. Summary of cooled NGV and un-cooled rotor measurements from the MT1 single stage high pressure turbine in the DERA isentropic light piston facility. Brite-EuRam TATEF project (BRPR-CT97-0519); 2002.

[11] Chana KS, Singh U. A programme to investigate the effects of film cooling in a high-pressure aeroengine turbine stage. Proc. of the Sixth European Conference on Turbomachinery – Fluid Dynamics and Thermodynamics 2005, March 7-11, Lille, France, Paper No. 079_05/58.

[12] Salvadori S, Montomoli F, Martelli F, Chana KS, Qureshi I, Povey T. Analysis on the effect of a nonuniform inlet profile on heat transfer and fluid flow in turbine stages. J Turbomach 2012, 134(1).